

Development and Evaluation of an AI System for Early Detection of Covid-19 Pneumonia using X-Ray

¹*Pooja.Hiremath, Student, Dept. of Information Science and Engineering, Dr Ambedkar Institute of Technology, Karnataka, India.*

²*Malathi.P, Assistant Professor Dept. of Information Science and Engineering, Dr Ambedkar Institute of Technology, Karnataka, India.*

Abstract – This work seeks to use artificial intelligence (AI) what's more, clinical science to foster a grouping instrument that can identify Covid-19 contaminations and other lung sicknesses. The four cases considered were Covid-19 pneumonia, non-Covid-19 pneumonia, pneumonia and summed up pneumonia. There are two phases for the proposed AI framework. Pneumocystis carinii is named pneumonia stage 1 chest X-ray volumes. Stage 2 uses information from Stage 1 to confirm whether the X-rays belong to the pneumonia category and classify them positively or generally using an in-deep learning framework.

Key Words: Corona Virus, Covid-19, Deep Learning.

1. INTRODUCTION

In-depth practice, which has grown into a major technology of artificial intelligence (AI), has been found to accurately diagnose lung diseases [1,2]. X-rays have been shown to be useful in the early stages of identifying and testing individuals with Covid-19. Our goal is to create a taxonomic framework that allows patients to classify chest x-ray images in two steps.

Stage 1 uses convulsive neural networks to classify X-rays as normal (healthy) patients and patients with pneumonia, while stage 2 uses convulsive neural networks to classify pneumonia patients as Covid-19 positive and Covid-19 negative (CNN). Patients with normal (healthy) lungs, pneumonia and existing patients were tested negative for Covid-19. The lower lobes of the brain are usually affected. Deep learning techniques can be used to assess patterns such as ground-glass opacity, uniformity, thick interlobular and interlobular septa [5,6]. In addition, the localization of pests improves care quality and any deviations that lead to complications are remotely monitored. Pleural effusion [7] is a common pathological diversion that requires immediate pressing of the pleura to relieve shortness of breath. As a result, our initiative seeks to reduce time, while at the same time improving our diagnostic skills.

2. IMPLEMENTATION OF SYSTEM

Image Collection:

The entire picture collection comprises 570 x-rays acquired from open image databases in 2018, as well as 369 positive Covid-19 images derived from 630 non-pulmonary x-rays and database open-ended images in SIRM and radiopaedia.org, which include X-ray reports of patients aged 25 to 67 years. In addition, the European Society of Radiology (ESR) database yielded 309 negative X-ray pictures of Covid-19.

Preparation of data:

The training data is properly treated to exclude severely degraded pictures that lower the trained model's accuracy. The data was given a ten percent rotation, a ten percent left and right shift, a ten percent height offset, and a twenty percent zoom. The X-ray picture was normalized using $1/225$. The training data set yielded a total of 15,024 X-ray pictures from the restricted data set after data improvement.

The proposed structure:

As shown in fig. In Figures 1 and 2, the proposed 2D CNN structure is used to identify patients infected with the Covid-19 virus from X-ray volumes [4]. The inlet structure, the middle flow and the exit flow are the three components of the whole structure. Portal flow is the first part of architecture, approving X-ray volumes, extracting features and sending them to flow between architectures.

Entry Flow

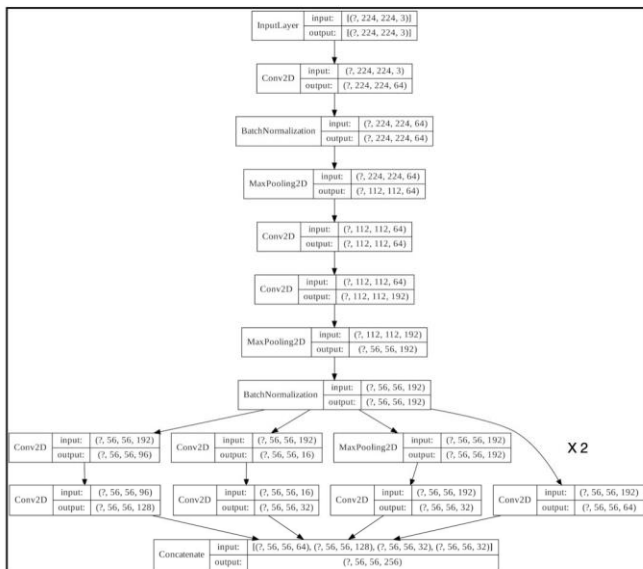


Fig 1: Architecture of CovAI-Net Entryflow

program. ResNet50 is a famous model from ResNet, and we took in a ton about its plan.

layer name	output size	18-layer	34-layer	50-layer	101-layer	152-layer
conv1	112x112	7x7, 64, stride 2				
conv2.x	56x56	3x3 max pool, stride 2				
		$\begin{bmatrix} 3 \times 3, 64 \\ 3 \times 3, 64 \end{bmatrix} \times 2$	$\begin{bmatrix} 3 \times 3, 64 \\ 3 \times 3, 64 \end{bmatrix} \times 3$	$\begin{bmatrix} 1 \times 1, 64 \\ 3 \times 3, 64 \\ 1 \times 1, 256 \end{bmatrix} \times 3$	$\begin{bmatrix} 1 \times 1, 64 \\ 3 \times 3, 64 \\ 1 \times 1, 256 \end{bmatrix} \times 3$	$\begin{bmatrix} 1 \times 1, 64 \\ 3 \times 3, 64 \\ 1 \times 1, 256 \end{bmatrix} \times 3$
conv3.x	28x28	$\begin{bmatrix} 3 \times 3, 128 \\ 3 \times 3, 128 \end{bmatrix} \times 2$	$\begin{bmatrix} 3 \times 3, 128 \\ 3 \times 3, 128 \end{bmatrix} \times 4$	$\begin{bmatrix} 1 \times 1, 128 \\ 3 \times 3, 128 \\ 1 \times 1, 512 \end{bmatrix} \times 4$	$\begin{bmatrix} 1 \times 1, 128 \\ 3 \times 3, 128 \\ 1 \times 1, 512 \end{bmatrix} \times 4$	$\begin{bmatrix} 1 \times 1, 128 \\ 3 \times 3, 128 \\ 1 \times 1, 512 \end{bmatrix} \times 8$
conv4.x	14x14	$\begin{bmatrix} 3 \times 3, 256 \\ 3 \times 3, 256 \end{bmatrix} \times 2$	$\begin{bmatrix} 3 \times 3, 256 \\ 3 \times 3, 256 \end{bmatrix} \times 6$	$\begin{bmatrix} 1 \times 1, 256 \\ 3 \times 3, 256 \\ 1 \times 1, 1024 \end{bmatrix} \times 6$	$\begin{bmatrix} 1 \times 1, 256 \\ 3 \times 3, 256 \\ 1 \times 1, 1024 \end{bmatrix} \times 23$	$\begin{bmatrix} 1 \times 1, 256 \\ 3 \times 3, 256 \\ 1 \times 1, 1024 \end{bmatrix} \times 36$
conv5.x	7x7	$\begin{bmatrix} 3 \times 3, 512 \\ 3 \times 3, 512 \end{bmatrix} \times 2$	$\begin{bmatrix} 3 \times 3, 512 \\ 3 \times 3, 512 \end{bmatrix} \times 3$	$\begin{bmatrix} 1 \times 1, 512 \\ 3 \times 3, 512 \\ 1 \times 1, 2048 \end{bmatrix} \times 3$	$\begin{bmatrix} 1 \times 1, 512 \\ 3 \times 3, 512 \\ 1 \times 1, 2048 \end{bmatrix} \times 3$	$\begin{bmatrix} 1 \times 1, 512 \\ 3 \times 3, 512 \\ 1 \times 1, 2048 \end{bmatrix} \times 3$
	1x1	average pool, 1000-d fc, softmax				
FLOPs		1.8x10 ⁹	3.6x10 ⁹	3.8x10 ⁹	7.6x10 ⁹	11.3x10 ⁹

As displayed above, the Resnet 50 design comprises of the accompanying parts:

- Warp with 7 * 7 portion sizes and 64 distinct parts, every 2 additions in size, bringing about a solitary layer.
- Next, we have most extreme gathering with 2 stage line.
- The following shows are 1 * 1, 64 centers, 3 * 3, 64 centers, and 1 * 1, 256 centers. These three layers are rehased multiple times altogether, for an aggregate of nine layers all through this period.
- Following that, there are 1 * 1, 128 centers, 3 * 3, 128 centers, and 1 * 1, 512 centers. This technique is rehased multiple times, adding up to 12 layers.
- Then there's the 1 * 1, 256 portion, 3 * 3, 256 piece, and 1 * 1, 1024 part, which are all rehased multiple times for a sum of 18 layers.
- Then 1 * 1, 512 centers in addition to 3 extra * 3, 512 centers and 1 * 1, 2,048 centers with a sum of nine layers.
- Next, we deal with the normal pool and end up with a layer that is completely connected with 1000 hubs and the Softmax work, giving us a solitary layer.
- Activation capacities and most extreme/normal pooling layers are not counted.
- As an outcome, we get a deep convolutional network with 1 + 9 + 12 + 18 + 9 + 1 = 50 layers.

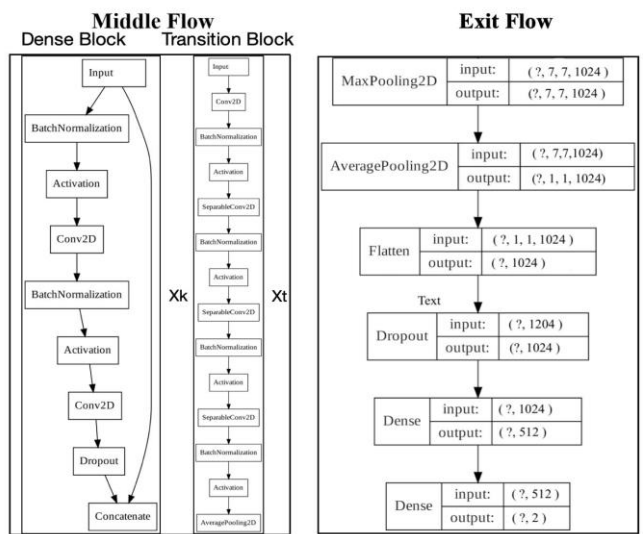


Fig 2: Architecture of CovAI-Net Middleflow and Exitflow

The proposed architecture, built on the carousel framework and using the tensor flow as its background, is inspired by three recent architectures: inception[8], densenet[10] and exclusion[11], and the selection of appropriate features such as smooth gradient flow from each of them. Fast twisting. The model is designed with 2D convulsions because it is easier to train with more training data, which leads to better accuracy.

ResNet50 is a res net with 48 transformation layers, one most extreme pool layer, and one normal pool layer. There are 3.8 x 10⁹ gliding point activities in this

Covid-19 Identification: To analyze pneumonia and Covid-19, we utilize two Resnet-50 examples.

3. BLOCK DIAGRAM

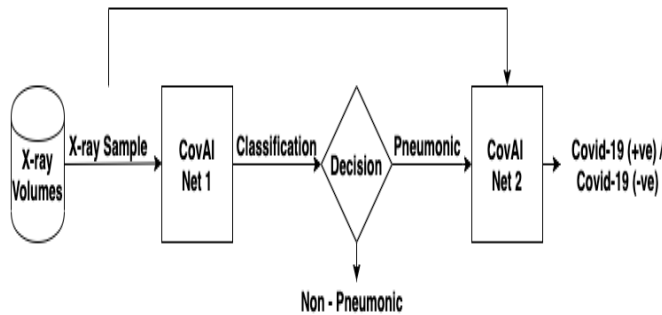


Fig 3: Workflow of CovAI System

The assessment of the experiment is shown in the diagram above in step-by-step phases. The X-ray dataset is imported first, and the data is sent into CovAI-Net1, which classifies the patient as having Pneumonia or being normal. If the patient develops Pneumonia again, the picture characteristics are sent to CovAI-Net2, which detects the Covid-19. It is also best explained and understandable by using flow chart along with schematic representation.

3.1. Schematic Representation of System

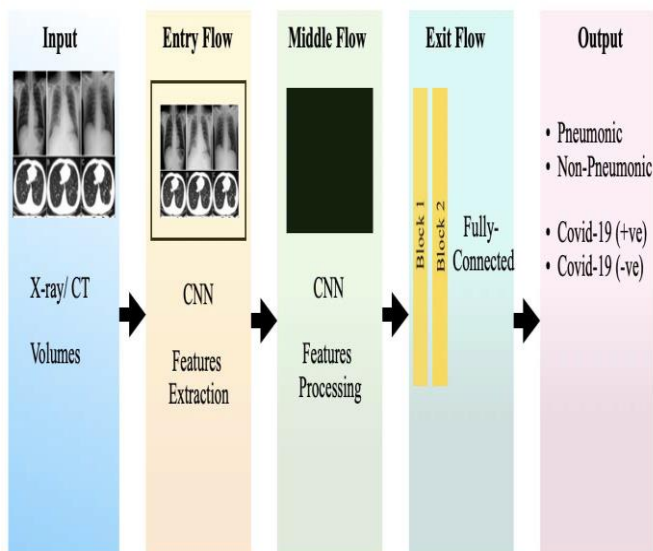
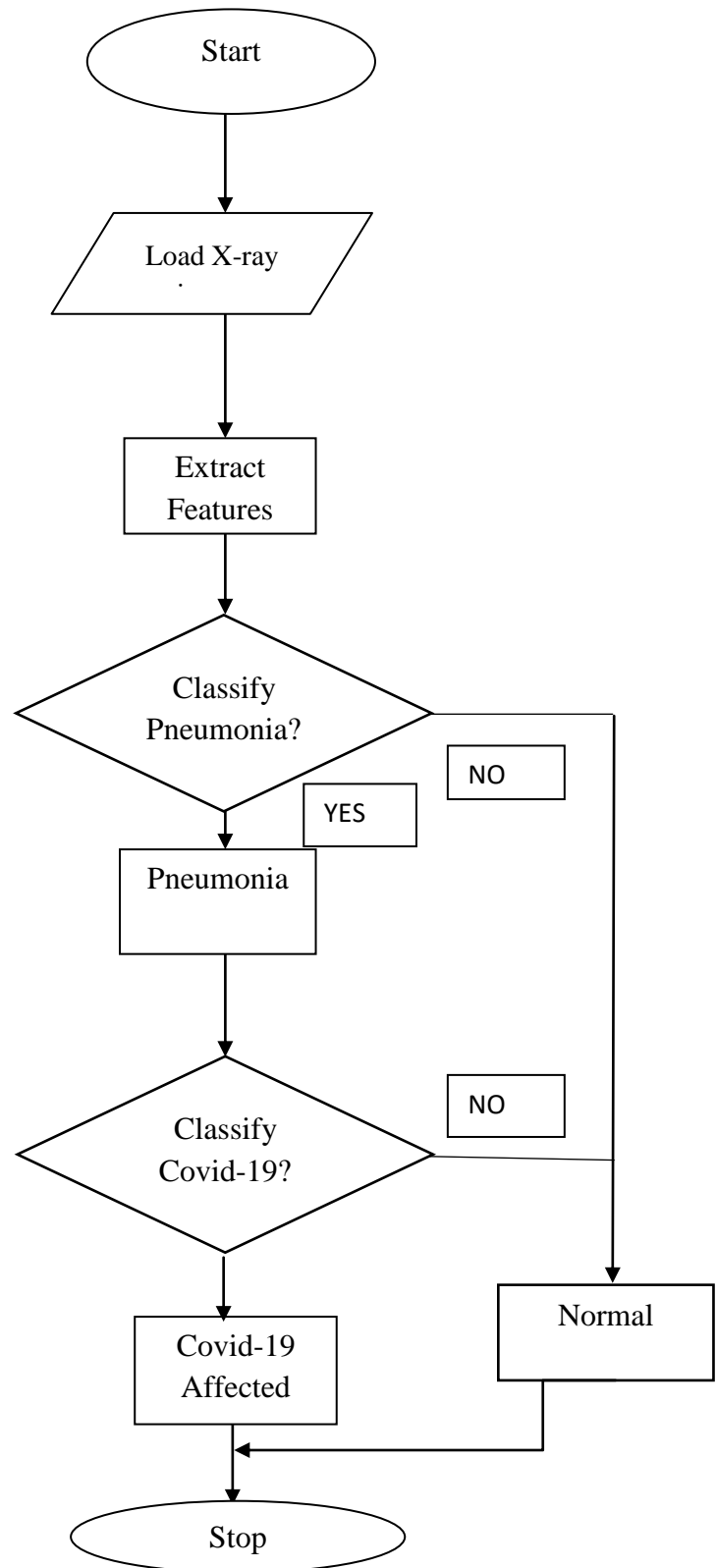


Fig 4: Schematic Representation of System

4. FLOW CHART



5. RESULT AND CONCLUSION

The last stage of a project is the outcome step, in which the system is assessed in terms of performance and the results are confirmed using graphs to see whether the project's objectives were fulfilled or not. A set of values is used to assess performance. A Confusion Matrix was used to assess the performances

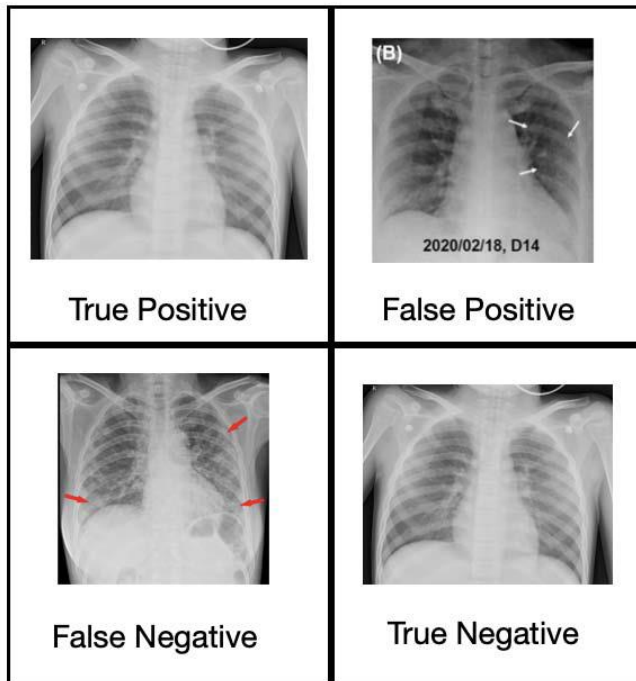


Fig 5:Outputs of Covid-19 positive and Covid-19 negatives test cases

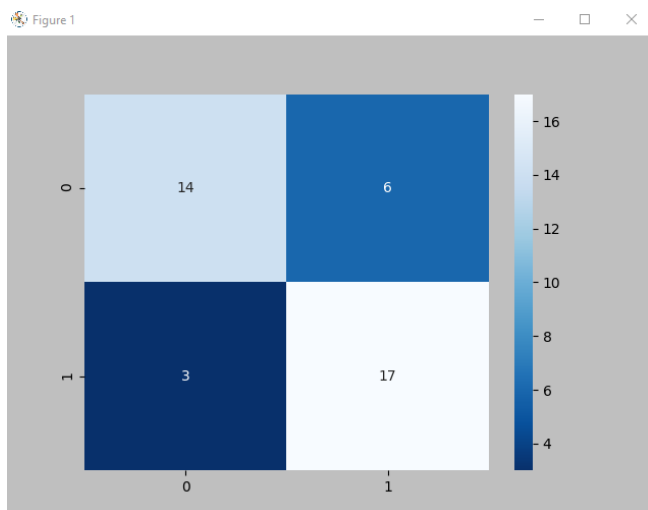


Fig 6:Graphical representation of Covid-19 positive and Covid-19 negative test cases

Due to a paucity of radiological data from Covid-19 virus-infected individuals, establishing CovAI -et is very challenging. To resolve this issue, information increase methods were utilized. Because of expanding responsibility, radiologists couldn't distinguish injuries in X-ray volumes, subsequently just X-ray volumes were sorted at the patient level (for example Coronavirus positive and Covid-19 negative).

The issue was tended to by considering the Covid-19 distinguishing proof issue as an ineffectively observed practice issue, that is, perceiving conceivable Covid-19 positive x-rays without indicating the Covid-19 sore areas. Gathering highlights from murky and obscured X-ray volumes is the third test. This issue was settled utilizing a part square of part design[15,16,17], which comprises of multi-dimensional centers that ensure ideal component extraction from X-ray volumes. The discoveries are probably going to be inaccurate since the ground glass darkness (GGO) in those photos is thick without combining. As an outcome, the recommended concentrate on fills in as a worldview and method for making a clinical man-made brainpower framework for testing and diagnosing Covid-19 sickness. Scientists have made the most dependable, non-obtrusive demonstrative method for identifying and diagnosing COVID-19 ailment utilizing man-made brainpower and clinical science.

6. ACKNOWLEDGEMENT

This research was supported by Dr.AIT college of engineering & technology. I am thankful to my guide Assistant Professor . Malathi .P who provided expertise that greatly assisted the research.

REFERENCES

[1] D. Shen, G. Wu, H. Suk. 2017 Deep learning in medical image analysis. Annu. Rev. Biomed. Eng. 19, 221-248. (doi:10.1146/annurev-bioeng-071516-044442).

[2] M. Anthimopoulos, S. Christodoulidis, L. Ebner, et al. Lung Pattern Classification for Interstitial Lung Diseases Using a Deep Convolutional Neural Network. IEEE Trans Med Imaging. 2016;35(5):1207-1216. (doi:10.1109/TMI.2016.2535865)

[3] J. Lei, J. Li, X. Li, et al. CT Imaging of the 2019 Novel Coronavirus (2019-nCoV) Pneumonia. Radiology 2020 Jan 31.

- [4] S. Albawi, T. A. Mohammed and S. Al-Zawi, "Understanding of a convolutional neural network," 2017 International Conference on Engineering and Technology (ICET), Antalya, 2017, page. 1-6.
- [5] N. Chen, M. Zhou, X. Dong, et al. Epidemiological and clinical characteristics of 99 cases of 2019 novel coronavirus pneumonia in Wuhan, China: a descriptive study [published January 29, 2020]. *Lancet*. (doi:10.1016/S0140-6736(20)30211-7)
- [6] S. Zhang, H. Li, S. Huang, et al. High-resolution CT features of 17 cases of corona virus disease 2019 in Sichuan province, China. *Eur Respir J* 2020. (doi: 10.1183/13993003.00334-2020)
- [7] H. Shi, X. Han, N. Jiang, et al. Radiological findings from 81 patients with COVID-19 pneumonia in Wuhan, China: a descriptive study. *Lancet Infect Dis*. 2020. ([https://doi.org/10.1016/S1473-3099\(20\)30086-4](https://doi.org/10.1016/S1473-3099(20)30086-4))
- [8] F. Chollet, "Keras", 2015 GitHub Repository, (<https://github.com/fchollet/keras>)
- [9] C. Szegedy, W. Liu, Y. Jia, et al., "Going deeper with convolutions," 2015 IEEE Conference on Computer Vision and Pattern Recognition (CVPR), Boston, MA, 2015, page. 1-9, (doi:10.1109/CVPR.2015.7298594).
- [10] G. Huang, Z. Liu, L. V.D. Maaten, et al. "Densely Connected Convolutional Networks," 2017 IEEE Conference on Computer Vision and Pattern Recognition (CVPR), Honolulu, HI, 2017, page. 2261-2269.
- [11] F. Chollet, "Xception: Deep Learning with Depthwise Separable Convolutions," 2017 IEEE Conference on Computer Vision and Pattern Recognition (CVPR), Honolulu, HI, 2017, page. 1800-1807.
- [12] Kingma, P. Diederik, B. Jimmy. Adam: A Method for Stochastic Optimization. arXiv:1412.6980 [cs.LG], December 2014
- [13] C. Nwankpa, W. Ijomah, A. Gachagan, et al. Activation functions: Comparison of trends in practice and research for deep learning. arXiv 2018, arXiv:1811.03378.
- [14] S. Bustin, T. Nolan. Pitfalls of quantitative real-time reverse-transcription polymerase chain reaction. *J Biomol Tech*. 2004;15(3):155-166.
- [15] D. Ardila, A.P. Kiraly, S. Bharadwaj, et al. Author Correction: End-to-end lung cancer screening with three-dimensional deep learning on low-dose chest computed tomography. *Nat Med* 25, 1319 (2019). (<https://doi.org/10.1038/s41591-019-0536-x>)
- [16] K. Suzuki. Overview of deep learning in medical imaging. *Radiol Phys Technol*. 2017; 10(3):257-273. (doi :10.1007/s12194-017-0406-5)
- [17] X. Wang., "A Weakly-supervised Framework for COVID-19 Classification and Lesion Localization from Chest CT," in *IEEE Transactions on Medical Imaging*, (doi: 10.1109/TMI.2020.2995965).
- [18] Z.-H. Zhou. A brief introduction to weakly supervised learning. *National Science Review*, 2017
- [19] J. Cheng, C. Weixiang, C. Yukun, et al. Artificial Intelligence Distinguishes COVID-19 from Community Acquired Pneumonia on Chest CT. *Radiology*, 2020. (<https://doi.org/10.1101/2020.03.20.20039834>)